substance: boron compounds with group III elements
property: properties of Al-B: α-AlB_{12}

Structure: tetragonal

Space group: $P4_12_12$ or $P4_32_12$ [94H].

The structure is based on B_{12} icosahedra and B_{20} units. The B_{20} units consist of two twinned icosahedra with a vacant apex on each side and a single B atom bridging both sides of the twinned icosahedra. All the linkages between those structural arrangements are formed along the quasi-fivefold axes of the B_{12} icosahedra or the corresponding directions of the twinned icosahedra. The Al atoms are statistically distributed on five crystallographic sites outside the B_{12} and B_{20} units. The occupancies of these sites vary between about 2 and 68 %.

Crystal chemistry of α-AlB_{12} and γ -AlB_{12} [99H1].

Preparation of α-AlB_{12} and γ -AlB_{12} [99H2].

lattice parameters
(in Å)

a	10.18(2)	*T* = 300 K	single crystal, X-ray diffraction	87K
c	14.343(10)			
a	10.16	*T* = 300 K	single crystal, X-ray diffraction	94H
c	14.26			
a	10.158(2)	*T*= 300 K	single crystal, X-ray diffraction	77H
c	14.270(5)			

pseudo-orthorhombic

a_p [201]	24.83	*T* = 300 K	87H2,
b_p [101]	17.52		85H,
c_p [010]	10.16		94W
V_p	4420 $Å^3$		

B_{12} icosahedral arrangement: Fig. 1; arrangement of B_{19} units: Fig. 2; nature of linkages between B_{12} and B_{19}: Fig. 3; nature of linkages between B_{12} and B_{19} through B: Fig. 4.

Arrangement of B_{12} icosahedra and B_{20} units in the structure of AlB_{12} in Fig. 5 and Fig. 6 [94H].

B_{19} unit in α-AlB_{12} as a result of the instability of the B_{12} icosahedral cluster and its rearrangement to a lower energy structure [91K1].

Average deformation of the electron densities in the bisecting plane of the icosahedron in Fig. 7 and the triangular face of the icosahedron in Fig. 8 [87H2, 94I].

Preparation by the high-temperature Al solution growth method in [94H].

Preparation by hot pressing [91K4].

Chemical properties of α-AlB_{12} of different dispersivity [87N].

position and occupancies of the Al atoms
(data from [77H, 77K])

Atoms	Position	Coordinates			Occupancies
		x	*y*	*z*	
Al_1	8(b)	0.3021(1)	0.3688(1)	0.2589(2)	71.7(7)
Al_2	8(b)	0.0823(1)	0.0118(1)	0.3086(1)	49.1(3)
Al_3	8(b)	0.3130(3)	0.3932(3)	0.3419 (4)	24.0(6)
Al_4	8(b)	0.2873(4)	0.4785(4)	0.1224(3)	15.0(3)
Al_5	8(b)	0.3037(35)	0.3831(43)	0.2958(91)	2.1(5)

Additional references to the data obtained from [77H, 77K]: [87H2, 87H1])

lattice constants of isotope enriched α-AlB_{12} (^{10}B: 90 % enriched; ^{11}B 99% enriched) [94H]
(in Å)

exp. No.	*a* (^{10}B)	*a*(^{11}B)	*a* (^{10}B) / *a*(^{11}B)	*c*(^{10}B)	*c*(^{11}B)	*c*(^{10}B) / *c*(^{11}B)
1	10.1579(4)	10.1559(4)	1.00020	14.2622(7)	14.2587(7)	1.00025
2	10.1568(5)	10.1539(5)	1.00029	14.2650(8)	14.2596(9)	1.00038
3	10.1598(3)	10.1586(2)	1.00012	14.2738(9)	14.2651(6)	1.00061

occupancies of Al sites in isotope enriched α-AlB_{12} (^{10}B: 90 % enriched; ^{11}B 99% enriched) [94H]
(in %)

	Al(1)	Al(2)	Al(3)	Al(4)	Al(5)
α-$Al^{10}B_{12}$	68.6(3)	47.3(3)	23.84	14.1(2)	2.24
α-$Al^{11}B_{12}$ (1)	69.3(3)	48.0(2)	24.44	14.0(2)	2.2(3)
α-$Al^{11}B_{12}$ (2)	68.5(2)	47.5(1)	24.2(1)	13.5(1)	1.9(2)

Electronic properties

For valence electron distribution, see Fig. 9.

Density of states calculation in Fig. 10 [94B]. For previous results of the same author, see [90B, 91B].

B K_α and Al $L_{2,3}$ spectra in [94G].

energy gaps
(in eV)

E_g	0.7(2)	T = 300 K	optical absorption	87H1
	1.1(2)	T = 300 K	optical absorption	
	1.75	T = 300 K	indirect allowed or non-direct	87G3
	1.95		indirect allowed or non-direct (new evaluation of data in Fig. 11)	
	0.24	T = 300 K	deep level	88W
	0.60		deep level	
	0.81		deep level	
	1.04		indirect allowed or non-direct	
	1.65		indirect allowed or non-direct	
	1.80		indirect allowed or non-direct	
	1.88		indirect allowed or non-direct	
	1.97		indirect allowed or non-direct	
	2.02		indirect allowed or non-direct	
	0.18	T = 100...192 K	electrical conductivity	87K
	0.23	T = 192...227 K		
	0.363	T = 227...357 K		
	1.9	T = 300 K	optical absorption	74G
	1.96	T = 300 K	optical absorption	79G
$E_{g,th}$	2.2	$T \geq$ 1000 K	electrical conductivity (intrinsic)	77B1, 74B

Low energy tail of the absorption edge of α-AlB_{12} (interpreted by the author as an Urbach tail) [91G1], absorption edge of α-AlB_{12} [87G3, 89G, 98W] and $(Al_{0.9}Be_{0.1})B_{12}$ [87G3, 89G] in Fig. 11.

Impurity and defects

activation energies

E_A	0.18...0.36 eV	T = 100...375 K	electrical conductivity	91P
	0.26...0.33 eV	T = 300 K	optical absorption	74G
	0.2...0.3 eV		electrical conductivity	73B

The behavior of hydrogen, nitrogen and oxygen impurities in aluminium dodecaboride (and boron carbide) for use as gas sensors is described in [91K3].

For the effect of doping with Be (compound $(Al_{0.9}Be_{0.1})B_{12}$) see Fig. 12 (optical absorption) and Fig. 13 (electrical conductivity) [87G3].

Lattice properties

IR active phonon wavenumbers

(ν/c) in cm^{-1}	430 480 565 600 650 710 785 905 1040 1180	T = 300 K	optical absorption (see Fig. 14), polycrystalline samples	74G
	1147 1125 1049 1030 1010 961 926 896 865 845 794 781 759 708 695 643 608 577 567 545 520 495 482 463 430 416 391 373 351 334 320 305 280 243 215 198 189 159 148 137 127 118 105 99 89 74 64	T = 300 K	obtained from the original data of the spectrum in Fig. 15	94W

Phonon absorption spectrum in Fig. 15 [94W].

Reflectivity spectrum in the phonon range in [87H1, 87W].

Poorly resolved absorption spectrum in the phonon range in [91P].

Raman spectrum of α-AlB_{12} in Fig. 16 [89G].

Poorly resolved IR and Raman phonon spectra of α-AlB_{12} in [91G2].

Transport properties

High temperature electrical conductivity and thermoelectric power in Fig. 17 [83G].

Low temperature resistivity in Fig. 18 [87G1, 87G2].

Temperature dependence of the electr. cond. of α-AlB_{12} compared with isostructural $Al_{0.9}Be_{0.1}B_{12}$ in Fig. 13 [87G3].

See also Figs. 17...23.

electrical conductivity
(in Ω^{-1} cm^{-1})

σ	$1.7 \cdot 10^{-1}$	T = 293 K		91P, 87K
	$10^{-2}...10^{-7}$	T = 300 K	polycrystalline samples; see also Figs. 19...21	79B, 74B, 77B1
	10^{-1}	T = 600 K	0.5 at% Mg doped, polycrystal	77B2
	$7 \cdot 10^{-2}$	T = 600 K	0.5 at% Zr doped, polycrystal	
	$3 \cdot 10^{-3}$	T = 600 K	0.5 at% Co doped, polycrystal	

For current-voltage characteristics, Hall coefficient and temperature dependence of resistance, see Figs. 20, 22, 23.

Current-voltage characteristics of α-AlB_{12} compared with $(Al_{0.9}Be_{0.1})B_{12}$ in [87G3].

Hot-pressed α-AlB_{12}: temperature dependence of the electrical conductivity (Fig. 24) and thermoelectric power (Fig. 25) [91K5].

Hot-pressed α-AlB_{12}: Effect of heating and cooling cycles on the electrical conductivity (Fig. 26) and on the thermoelectric power (Fig. 27) [91K5].

Effect of the porosity of hot-pressed samples on σ and S in [91K5].

Effect of Fe doping on the electrical conductivity in Fig. 28 and on the thermoelectric power in Fig. 29 [91K5].

thermoelectric powers

S	300...600 μV K^{-1}	T = 300 K	polycrystalline sample; see also Figs. 20, 21	74B, 77B1, 79B
	260 μV K^{-1}	T = 1000 K	0.5 at% Mg doped, polycrystal	77B2
	330 μV K^{-1}	T = 1000 K	0.5 at% Zr doped, polycrystal	
	400 μV K^{-1}	T = 1000 K	0.5 at% Co doped, polycrystal	
	200...350 μV K^{-1}	T = 900 K		91K5

Optical properties

dielectric constants

$\varepsilon(0)$	19	T = 300 K	questionable result, derived from reflectivity, see comment at Fig. 14	73B, 77B1
$\varepsilon(\infty)$	11	T = 300 K		

Further properties

thermal conductivity

κ	16.5(10) W $m^{-1}K^{-1}$	T = 300 K		91K2
	10.8(6) W $m^{-1}K^{-1}$	T = 1300 K		
	0.04 W cm^{-1} K^{-1}	T = 300 K	polycrystalline material. For temperature dependence, see Fig. 30	74B

Temperature dependence of the thermal conductivity in Fig. 31 [91K2, 91G3].

Temperature dependence of the thermal conductivity, influence of pores, in [91K2].

entropy

S	83.7(84) J $mol^{-1}K^{-1}$			86B

density

d	2.557...2.660 g cm^{-3}	T = 300 K	experimental	75S

melting point

T_m	2163°C			60G
	2070°C			75S

microhardness

H_K	2515 kg mm^{-2}	T = 300 K	100 g load, Knoop hardness	60G
	19.6(5) GPa		load 1.96 N	91P, 87K

fracture toughness

K_c	1.5(3) MN $m^{-3/2}$			91P, 87K

Strength and creep in aluminum dodecaboride(AlB_{12}) (and boron carbide (B_4C)) [99A].

References:

60G Giardini, A. A., Kohn, J. A., Toman, L., Eckart, D. W.: see [60E1], p. 140.

73B Berezin, A. A., Golikova, O. A., Zaitsev, V. K., Kazanin, M. M., Orlov, V. M., Stilbans, L. S., Tkalenko, E. N.: Sov. Phys. Solid State 15 (1973) 664.

74B Berezin, A. A., Golikova, O. A., Zaitsev, V. K., Kazanin, M. M., Orlov, V. M., Tkalenko, E. N.:Proc. 12th Int. Conf. Phys. Semicond. 1974, p. 291.

74G Golikova, O. A., Zaitsev, V. K., Orlov, V. M., Petrov, A. V., Tkalenko, F. N.: see [74G1], p. 25.

75S Samsonov, G. V., Serebryakova, T. I., Neronov, V. A.: Boridy, Moskva Atomizdat, 1975.

75Z Zaitsev, V. K., Golikova, O. A., Kazamrn, M. M., Orlov, V. M., Tkalenko, E. N.: Sov. Phys. Semicond. 9 (1976) 1372.

77B1 Berezin, A. A., Golikova, O. A., Zaitsev, V. R., Kazanin, M. M., Orlov, V. M., Tkalenko, E. N., in:Boron and Refractory Borides, (Matkovich V. 1., ed.) Springer: Berlin, Heidelberg, New York 1977, p. 52.

77B2 Bairamashvili, T. A., Golikova, O. A., Kekelidze, L. I., Orlov, V. M.: Sov. Phys. Semicond. 11 (1977) 451.

77H Higashi, I., Sakurai, T., Atoda, T.: J. Solid State Chem. 20 (1977) 67.

77K Kasper, J. S., Vlasse, M., Naslain, R.: J. Solid State Chem. 20 (1977) 281.

77S Spear, K. E.: see [77B1], p. 439.

79B Bairamashvili, I. A., Kekelidze, L. I., Golikova, O. A., Orlov, V. M.: J. Less-Common Met. 67 (1979) 461.

79G Golikova, O. A., Kazanin, M. M., Orlov, V. M., Tkalenko, E. N., Fedorov, M. I.: J. Less-Common Met. 67 (1979) 363.

83G Golikova, O.A., Samatov, S.: Phys. Status Solidi (a) 77 (1983) 449.

85H Hanke, G., Müller, K.: Surf. Sci. 152/153 (1985) 902.

86B Borovikova, M.S., Fesenko, V.V.: J. Less-Common Met. 117 (1986) 287. (Proc. 8th Int. Symp. Boron, Borides, Carbides, Nitrides and Rel. Compounds, Tbilisi, Oct. 8 - 12, 1984)

87G1 Golikova, O.A.: in: Novel Refractory Semiconductors, MRS Symp. Proc. Vol. 97, D. Emin, T.L. Aselage, C. Wood ed., Materials Research Soc.: Pittsburgh, 1987, p. 17.

87G2 Golikova, O.A.: Phys. Status Solidi (a) 101 (1987) 277.

87G3 Golikova, O.A., Kazanin, M.M.: Phys. Status Solidi (a) 103 (1987) K41.

87H1 Haupt, H., Werheit, H., Siejak, V., Kannengiesser, U., Higashi, I.: in: Proc. 9th Int. Symp. Boron, Borides and Rel. Compounds, University of Duisburg, Germany, Sept. 21 - 25, 1987, H. Werheit ed., University of Duisburg: Duisburg, 1987, p. 385.

87H2 Higashi, I., Ito, T.: in: Proc. 9th Int. Symp. Boron, Borides and Rel. Compounds, University of Duisburg, Germany, Sept. 21 - 25, 1987, H. Werheit ed., University of Duisburg: Duisburg, 1987, p. 41.

87K Kisly, P.S., Prikhna, T.A., Goutar, N.A., Podarevskaya, O.V.: in: Proc. 9th Int. Symp. Boron, Borides and Rel. Compounds, University of Duisburg, Germany, Sept. 21 - 25, 1987, H. Werheit ed., University of Duisburg: Duisburg, 1987, p. 273.

87N Neronov, V.A., Matasova, K.A., Serebryakova, T.I., Lyashenko, V.I., Dudnik, E.M.: in: Proc. 9th Int. Symp. Boron, Borides and Rel. Compounds, University of Duisburg, Germany, Sept. 21 - 25, 1987, H. Werheit ed., University of Duisburg: Duisburg, Germany, 1987, p. 305.

87W Werheit, H.: in: Proc. 9th Int. Symp. Boron, Borides and Rel. Compounds, University of Duisburg, Germany, Sept. 21 - 25, 1987, H. Werheit ed., University of Duisburg: Duisburg, 1987, p. 142.

88W Wood, C.: Rep. Prog. Phys. 51 (1988) 51.

89G Golikova, O.A., Sokolov, A.P., Amandshtshanov, H.: Fiz. Tverd. Tela (Solid State Physics) 31 (1989) 234.

90B Bullett, D.W.: in: The Physics and Chemistry of Carbides, Nitrides and Borides; NATO ASI Series E: Applied Sciences Vol. 185, R. Freer ed., Kluwer Academic Publishers: Dordrecht, 1990, p. 513.

91B Bullett, D.W.: AIP Conf. Proc. 231 (1991) 21, in: Boron-Rich Solids, Proc. 10th Int. Symp. Boron, Borides and Rel. Compounds, Albuquerque, NM 1990 (AIP Conf. Proc. 231), D. Emin, T.L. Aselage, A.C. Switendick, B. Morosin, C.L. Beckel ed., American Institute of Physics: New York, 1991, p. 21.

91G1 Golikova, O.A.: in: Boron-Rich Solids, Proc. 10th Int. Symp. Boron, Borides and Rel. Compounds, Albuquerque, NM 1990 (AIP Conf. Proc. 231), D. Emin, T.L. Aselage, A.C. Switendick, B. Morosin, C.L. Beckel ed., American Institute of Physics: New York, 1991, p. 108.

91G2 Golikova, O.A., Sokolov, A.P.: in: Boron-Rich Solids, Proc. 10th Int. Symp. Boron, Borides and Rel. Compounds, Albuquerque, NM 1990 (AIP Conf. Proc. 231), D. Emin, T.L. Aselage, A.C. Switendick, B. Morosin, C.L. Beckel ed., American Institute of Physics: New York, 1991, p. 347.

91G3 Gosset, D., Guery, M., Kryger, B.: in: Boron-Rich Solids, Proc. 10th Int. Symp. Boron, Borides and Rel. Compounds, Albuquerque, NM 1990 (AIP Conf. Proc. 231), D. Emin, T.L. Aselage, A.C. Switendick, B. Morosin, C.L. Beckel ed., American Institute of Physics: New York, 1991, p. 380.
91K1 Kawai, R., Weare, J.H.: J. Chem. Phys. 95 (1991) 1151.
91K2 Kekelidze, L.I., Bairamashvili, I.A., Kovtun, V.N., Petrov, I.I., Tavartkiladze, D.K.: in: Boron-Rich Solids, Proc. 10th Int. Symp. Boron, Borides and Rel. Compounds, Albuquerque, NM 1990 (AIP Conf. Proc. 231), D. Emin, T.L. Aselage, A.C. Switendick, B. Morosin, C.L. Beckel ed., American Institute of Physics: New York, 1991, p. 371.
91K3 Kervalishvili, P.D., Giorgaadze, K.A., Tabudsidze, M.L.: Sens. Actuators B (chemical) 5 (1991) 261.
91K4 Kharlamov, A.I., Loichenko, S.V.: in: Boron-Rich Solids, Proc. 10th Int. Symp. Boron, Borides and Rel. Compounds, Albuquerque, NM 1990 (AIP Conf. Proc. 231), D. Emin, T.L. Aselage, A.C. Switendick, B. Morosin, C.L. Beckel ed., American Institute of Physics: New York, 1991, p. 473.
91K5 Kharlamov, A.I, Loichenko, S.V.: in: Boron-Rich Solids, Proc. 10th Int. Symp. Boron, Borides and Rel. Compounds, Albuquerque, NM 1990 (AIP Conf. Proc. 231), D. Emin, T.L. Aselage, A.C. Switendick, B. Morosin, C.L. Beckel ed., American Institute of Physics: New York, 1991, p. 94.
91P Prikhna, T.A., Kisly, P.S.: in: Boron-Rich Solids, Proc. 10th Int. Symp. Boron, Borides and Rel. Compounds, Albuquerque, NM 1990 (AIP Conf. Proc. 231), D. Emin, T.L. Aselage, A.C. Switendick, B. Morosin, C.L. Beckel ed., American Institute of Physics: New York, 1991, p. 590.
94B Bullett, D.W.: Proc. 11th Int. Symp. Boron, Borides and Rel. Compounds, Tsukuba, Japan, August 22 - 26, 1993, Jpn. J. Appl. Phys. Series 10 (1994), p. 31.
94G Golikova, O.A., Domashevskaya, E.P., Kazanin, M.M., Terekhov, V.A.: Proc. 11th Int. Symp. Boron, Borides and Rel. Compounds, Tsukuba, Japan, August 22 - 26, 1993, Jpn. J. Appl. Phys. Series 10 (1994), p. 56.
94H Higashi, I., Kobayashi, M., Bobayashi, K., Lundström, T., Tergenius, L.-E., Ito, T.: Proc. 11th Int. Symp. Boron, Borides and Rel. Compounds, Tsukuba, Japan, August 22 - 26, 1993, Jpn. J. Appl. Phys. Series 10 (1994), p. 7.
94I Ito, T., Kasukawa, T., Higashi, I., Satow, Y.: Proc. 11th Int. Symp. Boron, Borides and Rel. Compounds, Tsukuba, Japan, August 22 - 26, 1993, Jpn. J. Appl. Phys. Series 10 (1994), p. 11.
94W Werheit, H., Krach, G., Kuhlmann, U., Higashi, I., Gurin, V.N., Korsukova, M.M.: Proc. 11th Int. Symp. Boron, Borides and Rel. Compounds, Tsukuba, Japan, August 22 - 26, 1993, Jpn. J. Appl. Phys. Series 10 (1994), p. 96.
98W Werheit, H., Higashi, I.: (to be published).
99A Abzianidze, T.G., Eristavi, A.M., Shalamberidze, S.O.: J. Solid State Chem. (1999) (Proc. 13th Int. Symp. Boron, Borides and Rel. Compounds, Dinard, France, Sept. 1999).
99H1 Higashi, I.: J. Solid State Chem. (2000) (Proc. 13th Int. Symp. Boron, Borides and Rel. Compounds, Dinard, France, Sept. 1999).
99H2 Higashi, I., Shishido, T., Narukawa, T., Iimuara, Y., Sugawara, T., Hukuda, T.: J. Solid State Chem. (2000) (Proc. 13th Int. Symp. Boron, Borides and Rel. Compounds, Dinard, France, Sept. 1999).

Fig. 1.

α-AlB_{12}. B_{12} icosahedral arrangement as seen along the *c* axis. The icosahedra are marked with the following symmetry codes: i(*x*,*y*,*z*); ii(-*x*,-*y*,1/2+*z*); iii(1/2–*y*,1/2+*x*,3/4+*z*); iv(1/2+*y*,1/2–*x*,1/4+*z*); v(*y*,*x*, –*z*); vi(–*y*,–*x*,1/2–*z*); vii(1/2–*x*,1/2+*y*,3/4–*z*); viii(1/2+*x*,1/2–*y*,1/4–*z*) [77H].

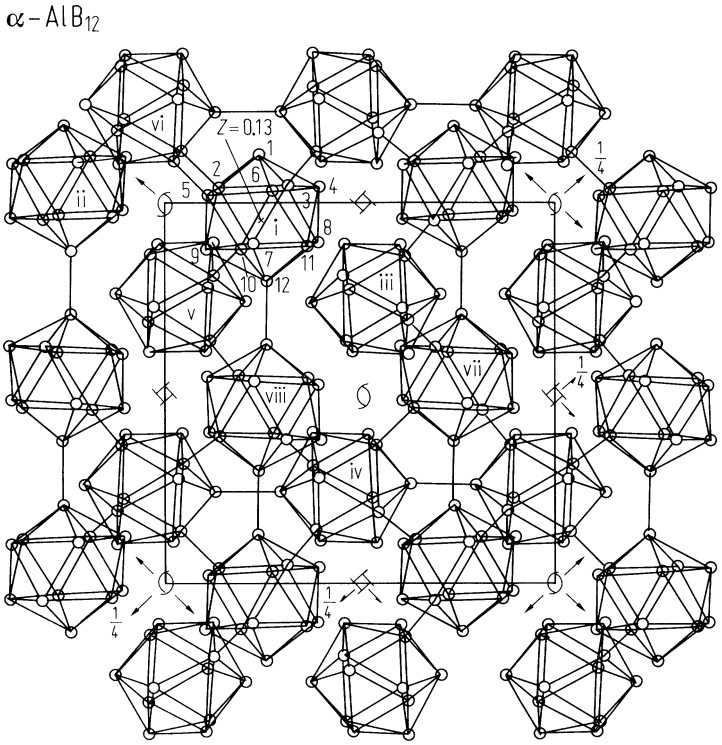

Fig. 2.

α-AlB_{12}. Arrangement of B_{19} units as seen along the *c* axis. The defect icosahedra involved in the B_{19} units are marked with the following symmetry codes: i, ii, iii, iv (see Fig. 1), v'(*y*,*x*,1–*z*), vi'(–*y*,–*x*,3/2–*z*), vii'(1/2–*x*,1/2+*y*,7/2–*z*), viii(1/2+*x*,1/2–*y*,3/4–*z*) [77H].

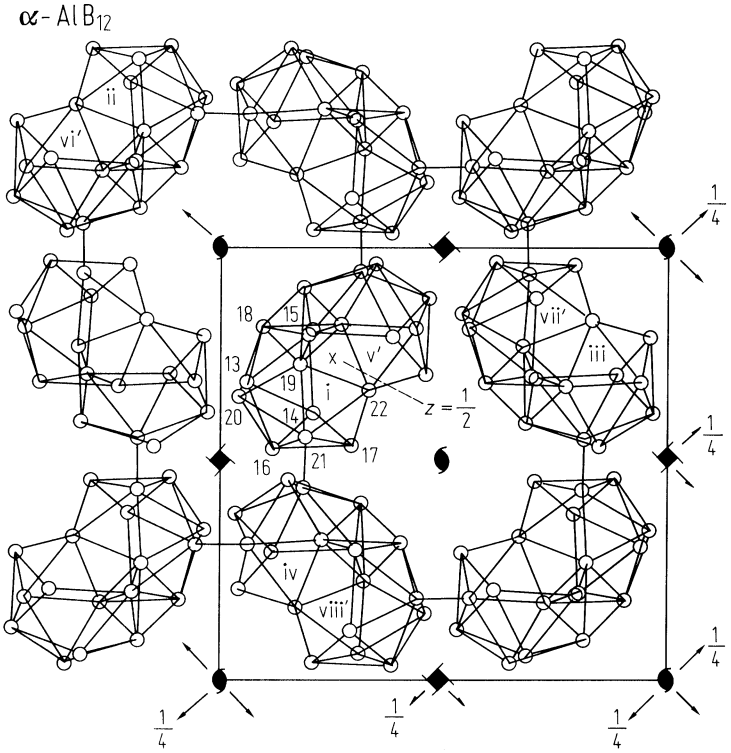

1

Fig. 3.

α-AlB_{12}. The nature of the linkages between B_{12} icosahedra and B_{19} units as projected on the (102) plane along the [101]-axis. The icosahedron defect icosahedra involved in B_{19} units and the B atoms, B(23) and B(5), are marked with following symmetry codes, where i, iv, vii and viii and v' are identical to those used in Figs. 1 and 2, respectively: i, ii'(1–*x*,–*y*,–1/2+*z*), ii"(1–*x*,1–*y*,–1/2+*z*), iii'(1/2–*y*,–1/2+*x*,–1/4+*z*), iii"(1/2–*y*,1/2+*x*,–1/4+*z*), iv,iv'(1/2+*y*,1/2–*x*,–3/4+*z*), v',vi"(1–*y*,–*x*,1/2–*z*), vi'"(1–*y*,1–*x*,1/2–*z*), vii, vii'(1/2–*x*,–1/2+*y*,3/4–*z*), viii [77H].

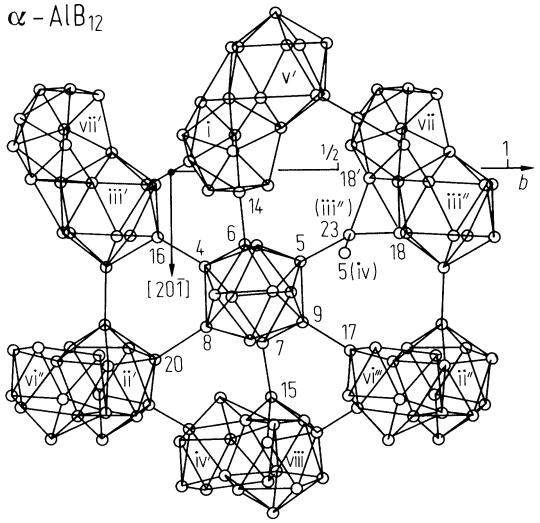

Fig. 4.

α-AlB_{12}. The nature of the linkage between a B_{12} icosahedron and a B_{19} unit through an intermediary single B atom as seen along the *c* axis. These units are marked with the symmetry codes which are identical to those used in Figs. 2 and 3 [77H].

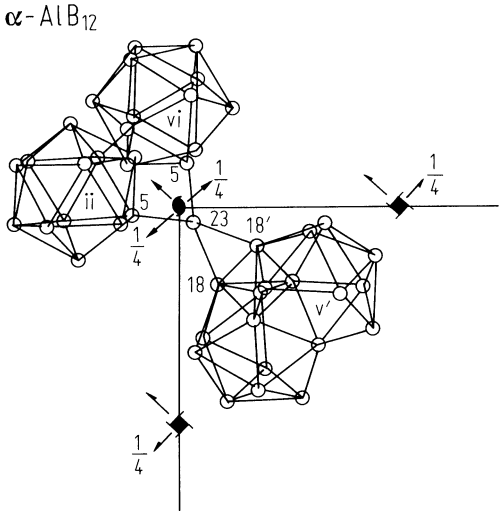

Fig. 5.

α-AlB_{12}. Arrangement of B_{12} icosahedra viewed down the *c* axis. There are $B_{12} - B_{12}$ linear chains along the *a* axis and $B_{12} - B_{12}$ spirals along the *c* axis [94H].

α-AlB_{12}

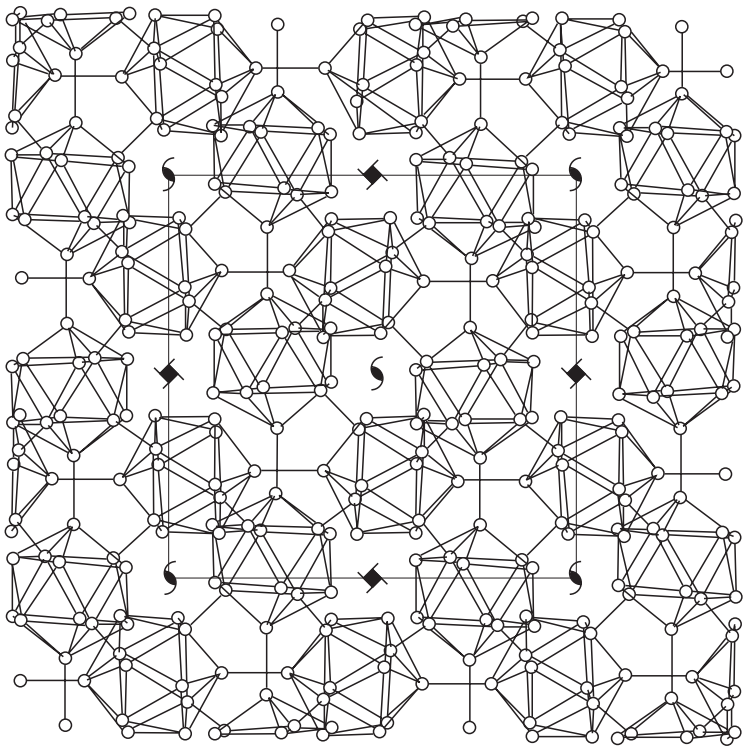

Fig. 6.

α-AlB_{12}**.** Arrangement of B_{20} units viewed down the *c* axis. There are B_{20} zig-zag chains along the *a* axis and $B_{20} - B_{20}$ spirals along the *c* axis [94H].

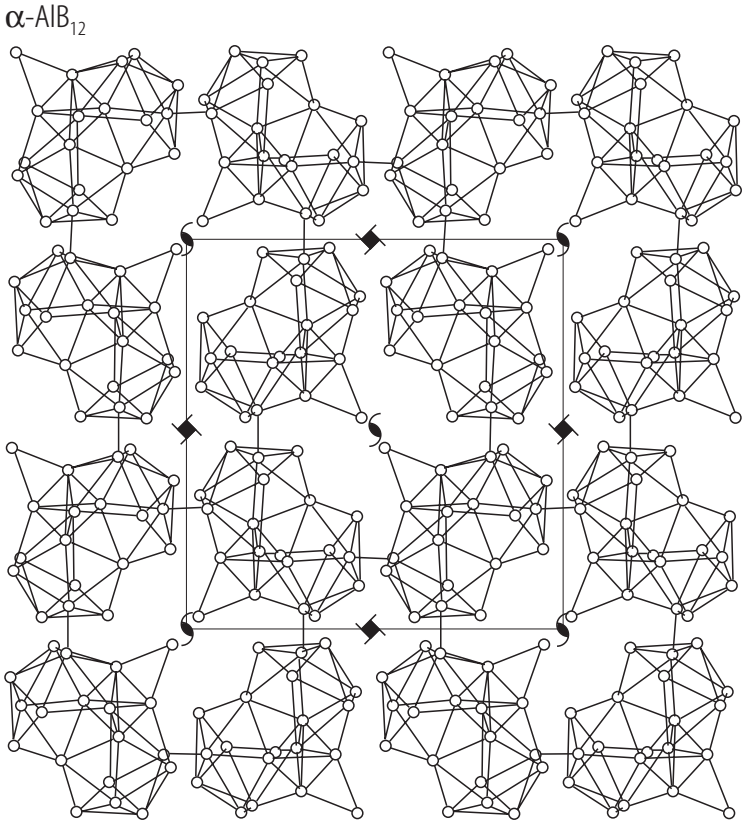

Fig. 7.

α-AlB_{12}. Average deformation of the electron density in the bisecting plane of the icosahedron in α-AlB_{12}. Contours at 0.025 eÅ^{-3}, negative contours dotted [94I].

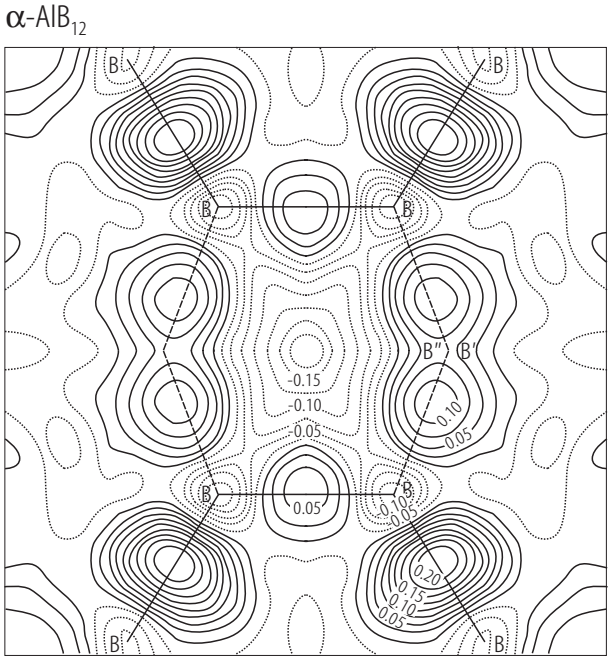

Fig. 8.

α-AlB_{12}. Average deformation of the electron density in the triangular face of the icosahedron in α-AlB_{12}. Contours at 0.025 eÅ^{-3} [87H2, 94I].

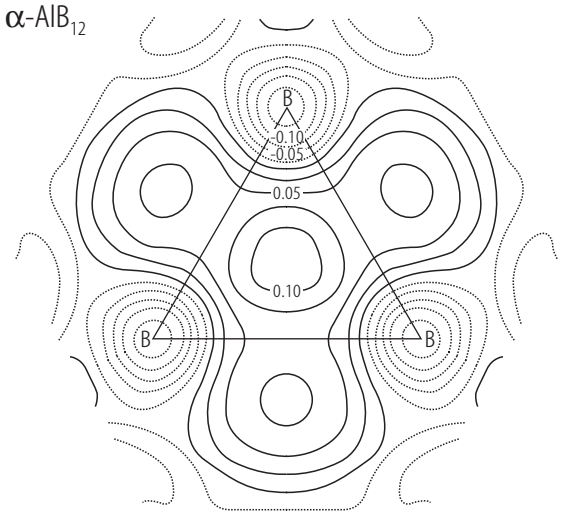

Fig. 9.

α-AlB_{12}. a) Averaged difference Fourier map through the bisecting plane of the icosahedron. Contours as in Fig. 2. Refer to Fig. 1 for the geometry. The four external B–B bonds lie on the plane. b) Difference Fourier map through the open pentagonal face of the B_{19} unit. Al(1)-Al(5)-Al(3) sites with the occupancies 0.717, 0.021 and 0.240, respectively are approximately 1.8 Å above the face. Contours as in Fig. 2 [77H]. Electron density in $eÅ^{-3}$.

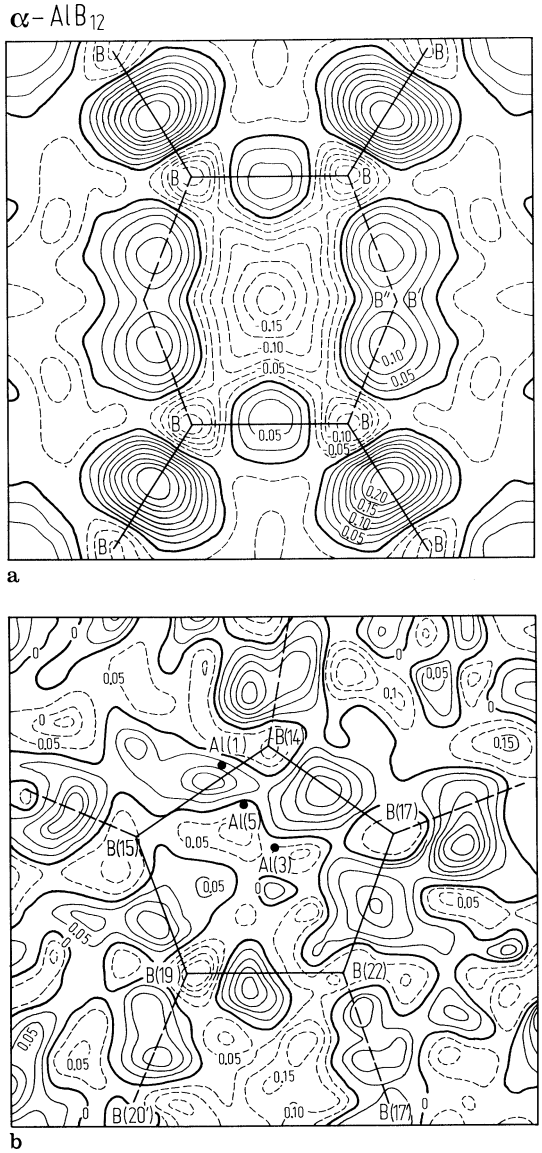

Fig. 10.

α-AlB_{12}. Energy distribution of electron states in AlB_{12} [94B].

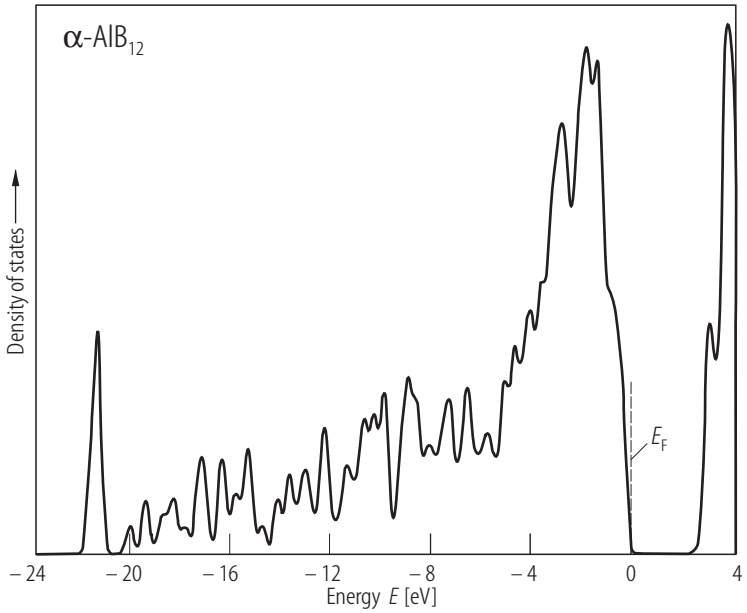

Fig. 11.

α-AlB_{12}. Absorption coefficient vs. photon energy in the absorption edge range. Golikova et al.:full triangles down: α-AlB_{12} [91G1], open triangles down: α-AlB_{12} [87G3, 89G]; full triangles: α-AlB_{12} (scaling of the ordinate as assumed to be correct because in the original paper it is obviously incorrect); Werheit et al. [98W] (at higher photon energies results of two different samples).

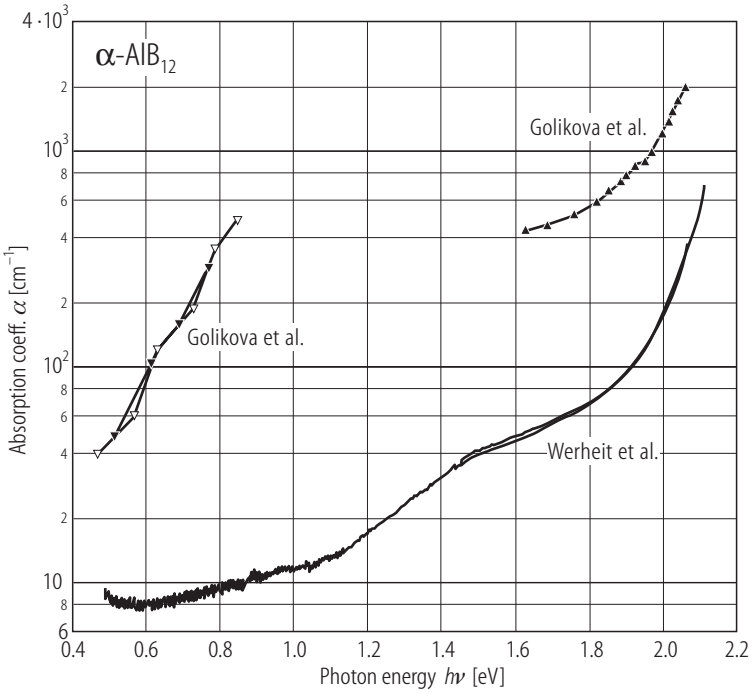

Fig. 12.

$Al_{1.2}$ $Be_{0.5}$ B_{22}. Absorption edge; absorption coefficient α vs. photon energy [87H1]; open circles, $Al_{0.9}Be_{0.1}B_{12}$ (scaling of the ordinate as assumed to be correct because in the original paper it is obviously incorrect) [87G3].

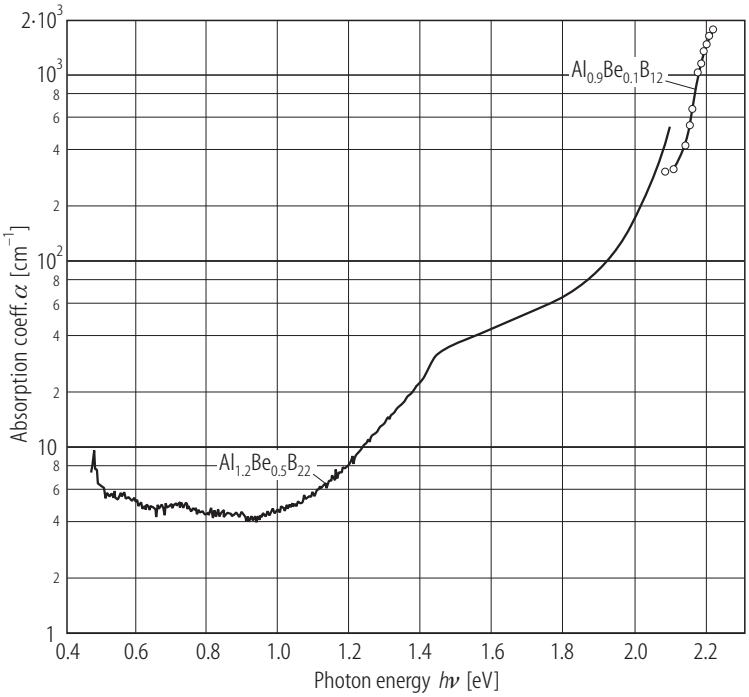

Fig. 13.

α-AlB_{12}, $(Al_{0.9}Be_{0.1})B_{12}$. Electrical conductivity vs. reciprocal temperature [87G3].

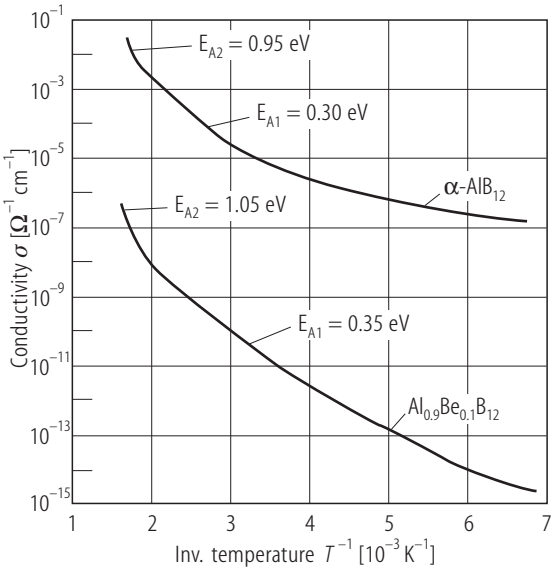

Fig. 14.

α-AlB_{12}. Absorption coefficient and reflectivity vs. wavenumber. Curve *1*. Sample with 10^2 Ω cm resistivity; curve *2*: Sample with 10^6 Ω cm resistivity (Remark: the strong increase of the reflectivity with increasing wavelength cannot be explained by lattice vibrations of such low oscillator strengths. Hence $\varepsilon(0)$, which has been derived from *R* should be put in question, too) [74B, 73B, 77B1].

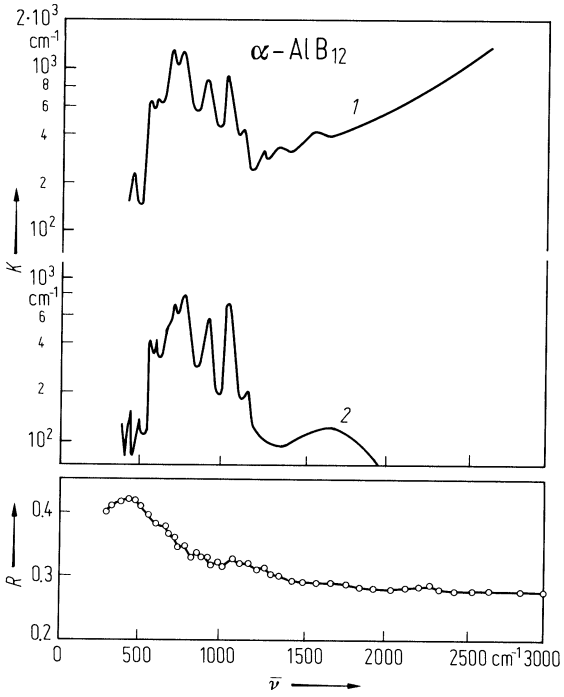

Fig. 15.

α-AlB_{12} and $Al_{1.2}$ $Be_{0.5}$ B_{22}. Phonon absorption spectra. Absorption index vs. wavenumber [94W].

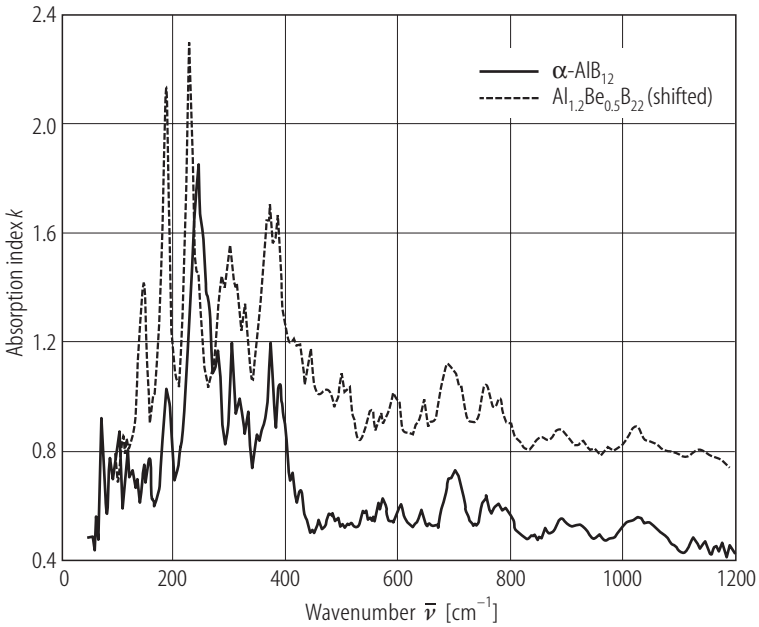

Fig. 16.

α-AlB_{12}. Raman spectrum, intensity vs. wavenumber [89G].

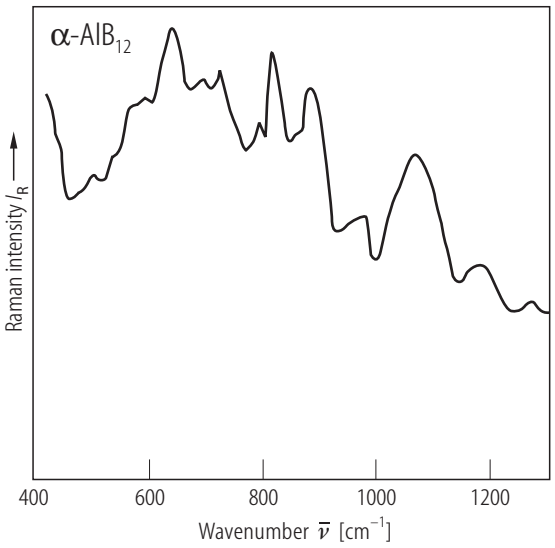

Fig. 17.

α-AlB_{12}. High temperature **(a)** electrical conductivity (σ vs. 1/T) and **(b)** thermoelectric power (S vs. T) [83G].

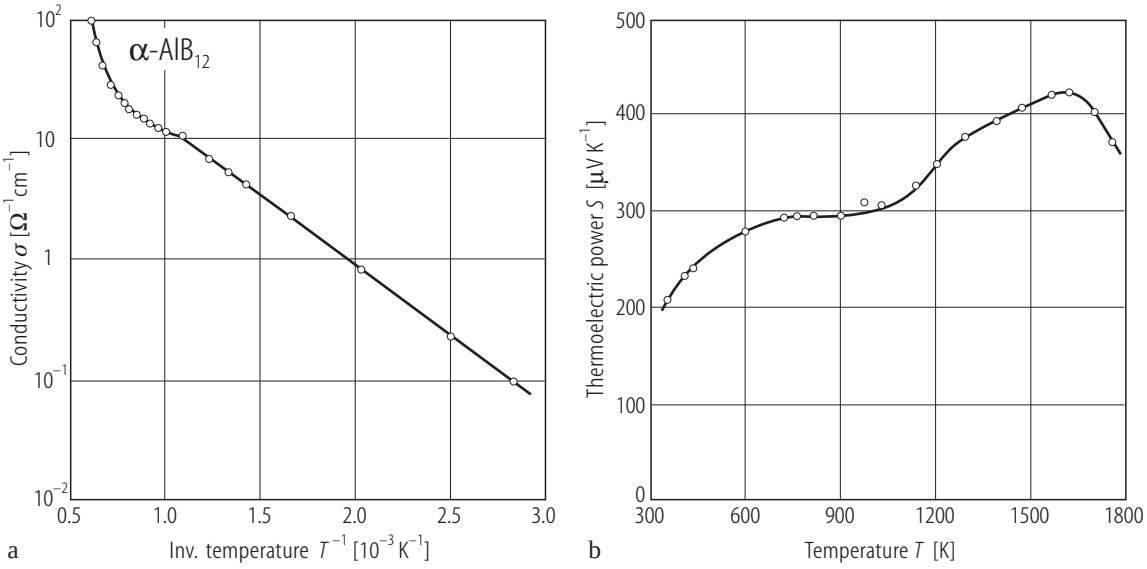

Fig. 18.

α-AlB_{12}. Low temperature electrical resistivity [87G1].

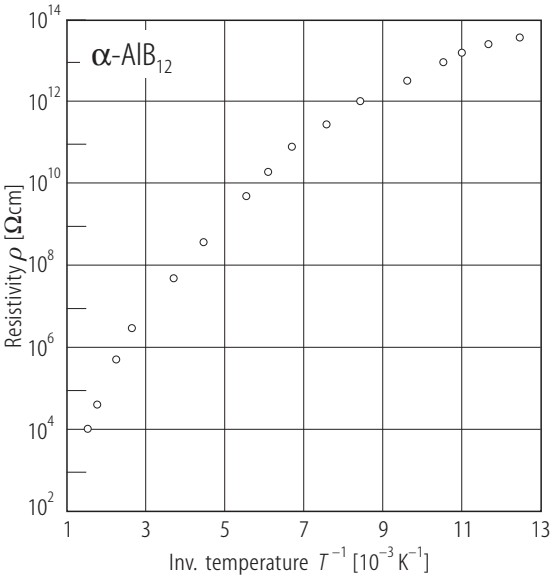

Fig. 19.

α-AlB_{12}. Conductivity of unspecified different polycristalline samples a) vs. reciprocal temperature, b) vs. $T^{-1/4}$ (according to Mott's law) [74B, 77B1].

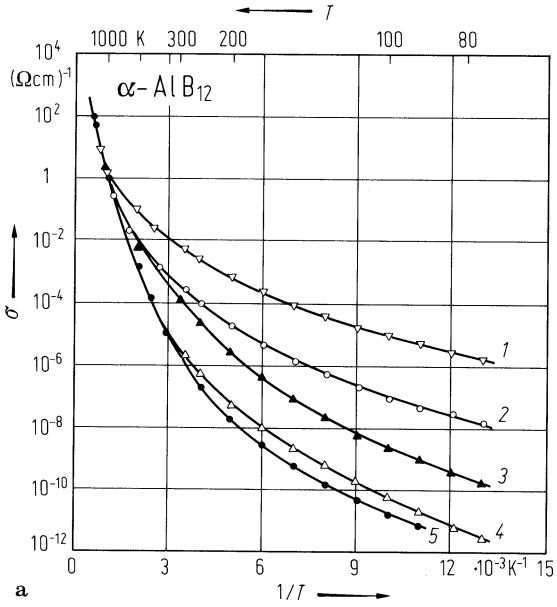

Fig. 20.

α-AlB_{12}. Conductivity, Hall coefficient and thermoelectric power of polycrystalline samples vs. reciprocal temperature [74B].

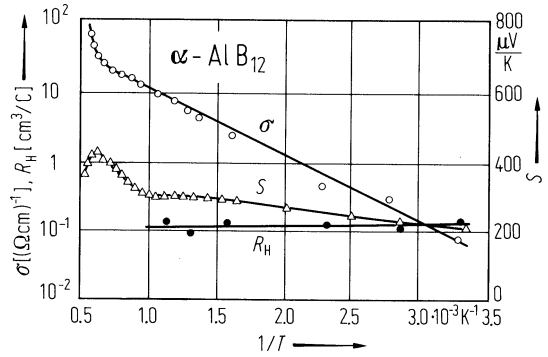

Fig. 21.

α-AlB_{12}. a) Conductivity vs. reciprocal temperature. b) Thermoelectric power vs. temperature. Curve *1*: single crystal (orientation unknown); curve *2*: pressed sample.

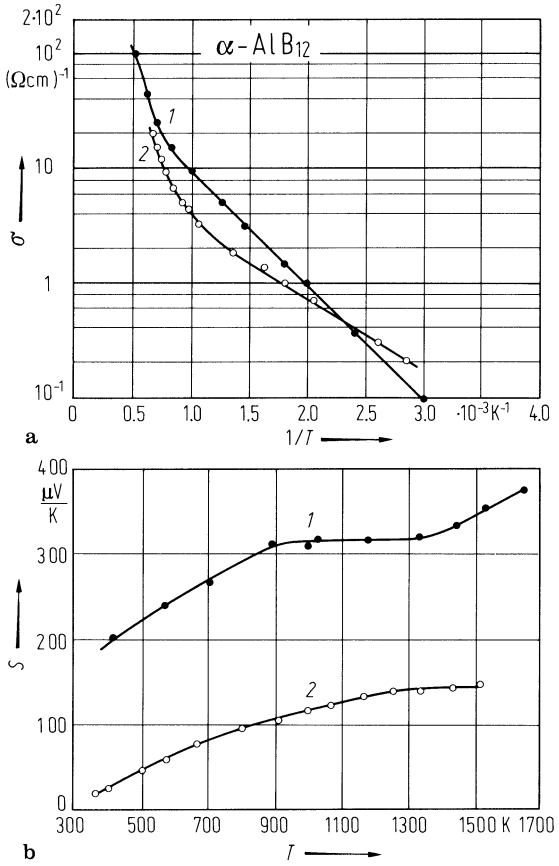

Fig. 22.

α-AlB_{12}. Current-voltage characteristics obtaine at 77 K in different states of a sample: Curves *1*: high-resistivity state, $I \propto \exp U^{1/2}$; *2*: intermediate state with a quadratic dependence; $I \propto U^2$; *3*: low-resistivity memory state, $I \propto U$ [75Z].

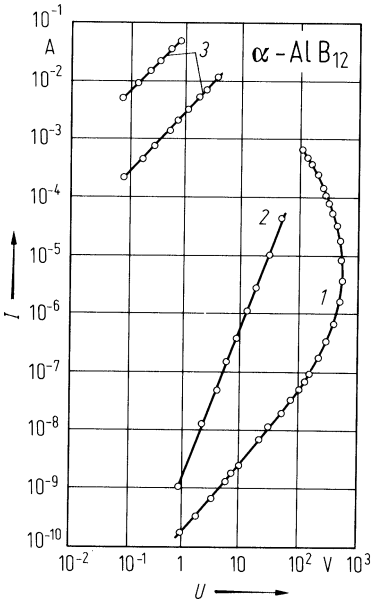

Fig. 23.

α-AlB_{12}. Resistance vs. reciprocal temperature in the low-resistivity memory state [75Z].

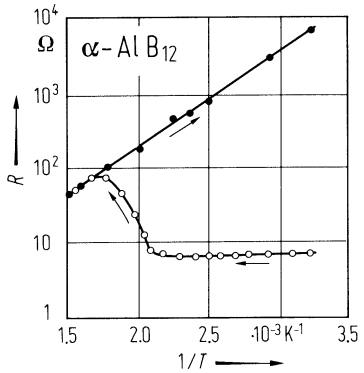

Fig. 24.

α-AlB_{12}. Temperature dependence of the electrical conductivity (σT vs. $1/T$) of hot-pressed α-AlB_{12}.[91K5].

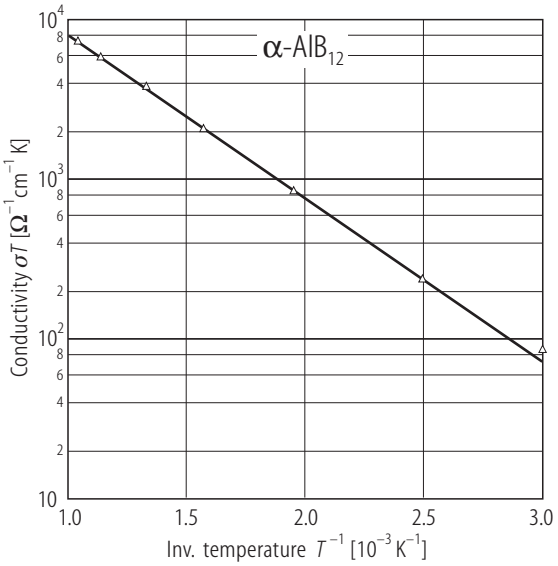

Fig. 25.

α-AlB_{12}. Temperature dependence of the thermoelectric power of hot-pressed α-AlB_{12} [91K5].

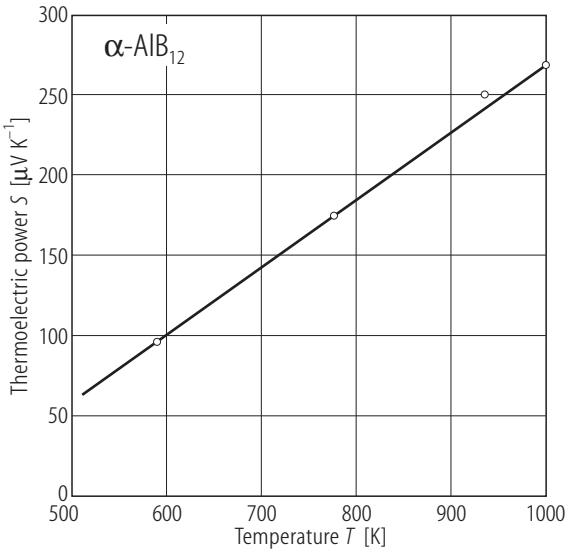

Fig. 26.

α-AlB_{12}. Effect of heating and cooling cycles on the electrical conductivity of hot-pressed α-AlB_{12}. 1st run: heating (open circles), cooling (open triangles); 2nd run: heating (diamonds), cooling (squares); 3rd run (after 2h annealing at 1800 K): heating (full circles), cooling (full triangles) [91K5].

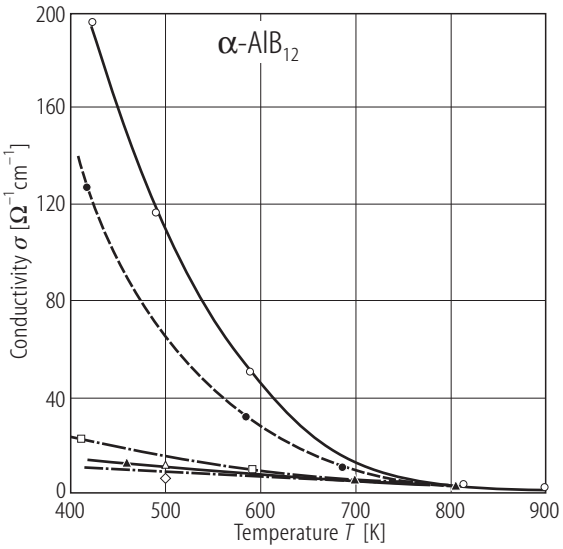

Fig. 27.

α-AlB_{12}. Effect of heating and cooling cycles on the thermoelectric power of hot-pressed α-AlB_{12}. 1st run: heating (open circles), cooling(open triangles); 2nd run: heating (diamonds), cooling (squares); 3rd run (after 2h annealing at 1800 K): heating (full circles), cooling (full triangles) [91K5].

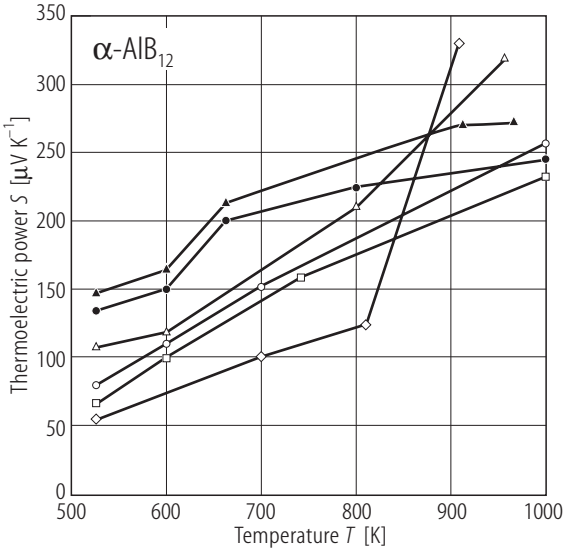

Fig. 28.

α-AlB_{12}.Electrical conductivity of Fe-doped α-AlB_{12}. (*1*) undoped; (*2*) 1.5 wt.% Fe; (*3*) 2.5 wt.% Fe [91K5].

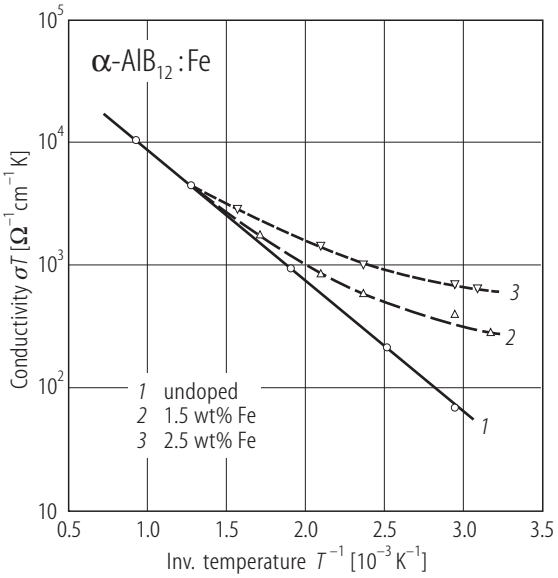

Fig. 29.

α-AlB_{12}.Thermoelectric power of Fe-doped α-AlB_{12} vs. Fe content at T = 800 K [91K5].

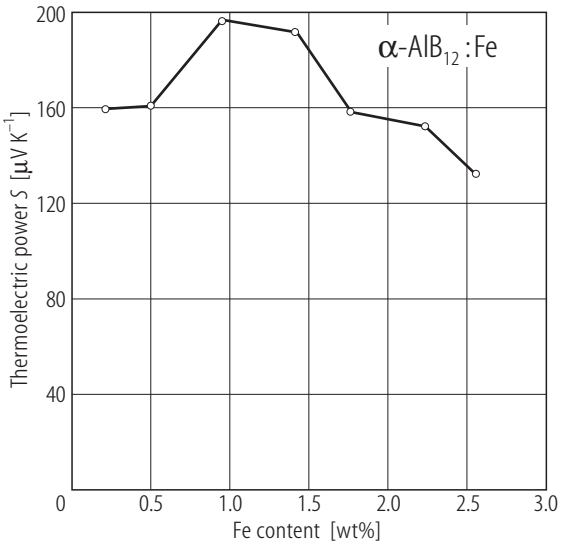

Fig. 30.

α-AlB_{12}. Thermal conductivity of polycrystalline samples vs. temperature [74B].

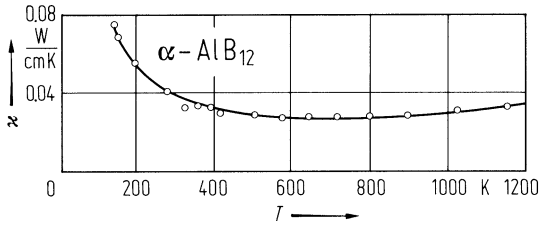

Fig. 31.

α-AlB_{12}.Thermal conductivity vs. *T*. Circles, experimental data, obtained by the extrapolation of measured data to eliminate the influence of pores caused by the preparation process (a linear relation between volume fraction of pores between about 50 and 75 % and thermal conductivity was experimentally proved). Full lines, selected calculations based on Callaway's phenomenological theory (for details, see reference) [91K2]; broken line, experimental result [91G3].